




## Article

# The Quasar CTD 135 is Not a Compact Symmetric Object

Sándor Frey <sup>1,2,\*</sup> , Krisztina É. Gabányi <sup>1,3,4</sup>  and Tao An <sup>5</sup> 

- <sup>1</sup> Konkoly Observatory, Research Centre for Astronomy and Earth Sciences, Konkoly Thege Miklós út 15-17, H-1121 Budapest, Hungary; k.gabanyi@astro.elte.hu
- <sup>2</sup> Institute of Physics, ELTE Eötvös Loránd University, Pázmány Péter sétány 1/A, H-1117 Budapest, Hungary
- <sup>3</sup> Department of Astronomy, Institute of Geography and Earth Sciences, ELTE Eötvös Loránd University, Pázmány Péter sétány 1/A, H-1117 Budapest, Hungary
- <sup>4</sup> ELKH-ELTE Extragalactic Astrophysics Research Group, ELTE Eötvös Loránd University, Pázmány Péter Sétány 1/A, H-1117 Budapest, Hungary
- <sup>5</sup> Shanghai Astronomical Observatory, Key Laboratory of Radio Astronomy, Chinese Academy of Sciences, 80 Nandan Road, Shanghai 200030, China; antao@shao.ac.cn
- \* Correspondence: frey.sandor@csfk.org

**Abstract:** The radio-loud quasar CTD 135 (2234+282, J2236+2828) has been proposed as a candidate compact symmetric object (CSO), based on its symmetric radio structure revealed by multi-frequency very long baseline interferometry (VLBI) imaging observations on milliarcsec angular scales. CSOs are known as young jetted active galactic nuclei (AGN) whose relativistic plasma jets are misaligned with respect to the line of sight. The peculiarity of CTD 135 as a CSO candidate was its detection in  $\gamma$ -rays, while the vast majority of known  $\gamma$ -ray emitting AGN are blazars with jets pointing close to our viewing direction. Since only a handful of CSOs are known as  $\gamma$ -ray sources, the unambiguous identification of a single candidate is important for studying this rare class of objects. By collecting and interpreting observational data from the recent literature, we revisit the classification of CTD 135. We present evidence that the object, based on its flat-spectrum radio core with high brightness temperature, variability at multiple wavebands, and infrared colours should be classified as a blazar rather than a CSO.

**Keywords:** active galactic nuclei; blazars; compact symmetric objects; very long baseline interferometry;  $\gamma$ -rays; jets; variability

## 1. Introduction

Compact symmetric objects (CSOs) are physically small (<1 kpc) jetted active galactic nuclei (AGN) with powerful radio emission. As their name coined by [1] indicates, they show a symmetric “mini-lobe” structure around a central core. The core itself often remains weak or even undetected in high-resolution very long baseline interferometry (VLBI) imaging because the jets originating from the vicinity of the central supermassive black hole are inclined to the line of sight by a large angle. It is in sharp contrast with blazars, where jets nearly align with the viewing direction. The synchrotron radio emission of blazar jets is enhanced by relativistic beaming, while the emission of CSOs is dominated by the shock fronts where the energetic jets interact with the ambient material.

When monitored with VLBI, blazars typically show apparent superluminal jet component motion, a combined effect of a plasma outflow whose speed is intrinsically close to the speed of light, and the small jet inclination [2]. On the other hand, the apparent hotspot expansion speed in CSOs is mostly subluminal. CSOs are known to represent the earliest evolutionary phase of symmetric jetted radio AGN [3–6].

arXiv:2202.00950v1 [astro-ph.GA] 2 Feb 2022



**Citation:** Frey, S.; Gabányi, K.É.; An, T. The Quasar CTD 135 is Not a Compact Symmetric Object. *Symmetry* **2022**, *1*, 0. <https://doi.org/>

Academic Editor: Firstname  
Lastname

Received:  
Accepted:  
Published:

**Publisher’s Note:** MDPI stays neutral with regard to jurisdictional claims in published maps and institutional affiliations.



**Copyright:** © 2022 by the authors. Licensee MDPI, Basel, Switzerland. This article is an open access article distributed under the terms and conditions of the Creative Commons Attribution (CC BY) license (<https://creativecommons.org/licenses/by/4.0/>).

Blazars are by far the most common AGN class found among the associated extragalactic objects in the most recent  $\gamma$ -ray source catalogue of the *Fermi* Large Area Telescope (LAT) [7]. However, there are theoretical works predicting  $\gamma$ -ray emission also from CSOs [8–10]. Only a handful of CSOs and somewhat more extended radio AGNs (e.g., [11]) with misaligned jets are known as  $\gamma$ -ray sources (see a recent review in [12] and references therein). The radiation mechanism and the exact location where the  $\gamma$ -rays come from are still under debate. Unlike for blazars, relativistic beaming in jets cannot be dominant. Instead, isotropic high-energy emission from the expanding lobes was predicted by [8] from studying the evolution of ultra-relativistic electrons injected from a terminal hotspot. Inverse-Compton scattering of seed photons by relativistic electrons in the jets was also proposed as a possible mechanism of non-thermal high-energy emission [10]. On the other hand, a thermal origin, free-free emission from the shocked plasma may also lead to  $\gamma$ -ray emission in CSOs [9]. Among the few confirmed  $\gamma$ -ray CSOs, PKS 1718–649 at low redshift ( $z = 0.014$ ) and with only  $\sim 100$  yr kinematic age may produce  $\gamma$ -rays via inverse-Compton scattering of the ambient photon fields by non-thermal electrons in the radio lobe [13]. In case of NGC 3894 ( $z = 0.011$ ), another very young CSO, the jet origin cannot be excluded [14]. Owing to the small number of such sources known to date, secure identification of any additional  $\gamma$ -ray-emitting CSO or larger medium-sized symmetric object (MSO) could provide a valuable test for models of (non-beamed)  $\gamma$ -ray emission in AGN.

The quasar CTD 135 (2234 + 282, J2236 + 2828) emerged as a promising candidate, as it is associated with a *Fermi* source (4FGL J2236.3 + 2828, [7]), its radio morphology observed with cm-wavelength VLBI imaging at multiple frequencies is reminiscent of a CSO, and its radio spectrum based on total flux density measurements appears to peak at around 1 GHz [15]. However, determining the shape of the radio spectrum could be uncertain if the source is highly variable in time and the flux density measurements are not simultaneous. The spectroscopic redshift of CTD 135 is  $z = 0.790$ . Its optical spectrum is characteristic of blazars in a bright continuum-dominated state, but a broad Mg II emission line with observed-frame equivalent width of  $4.9 \text{ \AA}$  was detected in the spectrum in a low state [16]. Therefore the optical spectrum is transitional between flat-spectrum radio quasars (FSRQs) and BL Lac objects, affected by flux variability [16].

The peaked radio spectrum, the nearly symmetric, compact sub-kpc morphology, the absence of Doppler-boosted radio emission, and the slowly advancing component motion in CSOs [17] are consistent with misaligned, young jetted radio sources. In sharp contrast, blazars typically have flat or inverted radio spectra, a one-sided core–jet structure, a compact core with high brightness temperature, indicating Doppler boosting in a jet closely aligned with the line of sight, and often apparent superluminal expansion speed.

However, relativistically beamed radio AGN could sometimes be confused with CSOs, if structural information is considered only. A typical core–jet morphology with a relatively bright jet component could mimic a compact double source [18]. For a more secure CSO classification, it is desirable to apply further selection criteria in addition to the classical ones, by investigating radio flux density variability, and the apparent separation speed between emission features seen in VLBI images with milliarcsec (mas) angular resolution [18]. In general, sources with beamed jets are expected to show rapid and high-amplitude flux density variability, as opposed to misaligned radio AGN. The apparent advance speed of CSO hotspots is generally lower than the core–jet separation speed derived from the jet component proper motions in blazars. Both criteria above require a long series of radio observations, either flux density monitoring, or multi-epoch VLBI imaging at a given frequency.

Another potential diagnostic tool is offered by the precise optical astrometry enabled by the *Gaia* space mission [19]. The positional accuracy of *Gaia* is comparable to that available with VLBI observations in radio. Most of the optical emission from an AGN is associated with the accretion disk surrounding the central black hole, perhaps with some contribution from the

inner jet [20], but certainly not with the radio lobes. Therefore, a compact double radio source without a clearly detected central VLBI core, but with the *Gaia* optical position available and falling in between the two opposite hotspots, is a strong indication for a CSO [21].

A recent publication [22] gave a comprehensive analysis of the observed properties, in particular the  $\gamma$ -ray variability and broad-band spectral energy distribution (SED), of CTD 135. The authors assumed that the source is a typical CSO, but many findings of the study suggest that its properties are more consistent with a blazar. This contradiction motivated us to revisit the case of CTD 135 as a potential CSO candidate. In Section 2, we collect multi-band observational data relevant for the source classification. In the light of new observational evidence from multiple literature sources, we argue in Section 3 that the source is not a CSO.

## 2. Observational Data

### 2.1. High-Frequency VLBI Imaging

The primary classification criteria for a CSO are the presence of compact radio emission within a projected linear size of 1 kpc, and a symmetric compact double-lobed structure seen on both sides of a central source. Archival VLBI images at 2.3, 5, 8.4, and 15 GHz analyzed by [15] indicated a barely resolved source in the northeast–southwest (NE–SW) direction. Circular Gaussian brightness distribution model components fitted to the highest-resolution 15-GHz data suggested three distinct components. However, the central component, the putative core, was blended with the NE feature in all other images made at frequencies lower than 15 GHz.

At that time, no VLBI imaging data at higher frequencies, and thus with higher angular resolution, were available. The 15-GHz data used by [15] were obtained in the framework of the Monitoring of Jets in Active Galactic Nuclei with VLBA Experiments (MOJAVE) survey programme [23] performed with the U.S. Very Long Baseline Array (VLBA). CTD 135 was monitored in 25 epochs from 1995 to 2015 and the data are available in the survey website (<http://www.physics.purdue.edu/astro/MOJAVE/sourcepages/2234+282.shtml>, accessed: 2 February 2022). In a jet kinematic analysis of the first 19 years of 15-GHz MOJAVE observations, [24] interpreted the mas-scale source structure differently from [15], and assumed the NE component as the core of a blazar with a one-sided jet pointing to SW. Based on measurements at 7 epochs, [24] estimated the apparent jet component proper motion as  $3.26 \pm 0.30$  times the speed of light ( $c$ ), i.e., a superluminal value typical for blazars. In turn, the most recent jet kinematic analysis of the MOJAVE data [25] identified the core with the SW component, and estimated almost negligible proper motion,  $(0.58 \pm 0.53) c$ , from 8 epochs of VLBA data. The controversial proper motion estimates are the sign of the difficulties in reliably identifying jet features with less than 1 mas separation from the core in this source across the observing epochs at 15 GHz. Multi-epoch MOJAVE 15-GHz polarization measurements [26] indicate that the fractional linear polarization is typically higher (up to  $\sim 10\%$ ) in the NE component and lower or undetected in the SW component of CTA 135, suggesting the latter is the weakly polarized core.

The unambiguous identification of the core with the SW component was made possible by the 43-GHz VLBA image published by [27], as CTD 135 was included in the sample of 124 radio AGN observed in their survey. A naturally weighted image prepared from the same data in DIFMAP [28] is displayed in Figure 1. We constructed the spectral index image of the source and show it in Figure 2. It is based on the 43-GHz data obtained on 18 January 2016 [27] and the 15-GHz MOJAVE data from 19 December 2015. The epoch of the latter was chosen to be the closest in time to that of the 43-GHz image, to minimize the effect of possible variability. The colour scale indicates the spatial distribution of the two-point spectral index  $\alpha$ ; it is defined following the convention  $S \propto \nu^\alpha$ , where  $S$  is the brightness of the given image pixel and  $\nu$  the observing frequency. The spectral index image was constructed using the VIMAP [29] tool that allows us to properly align the images made at two different frequencies.

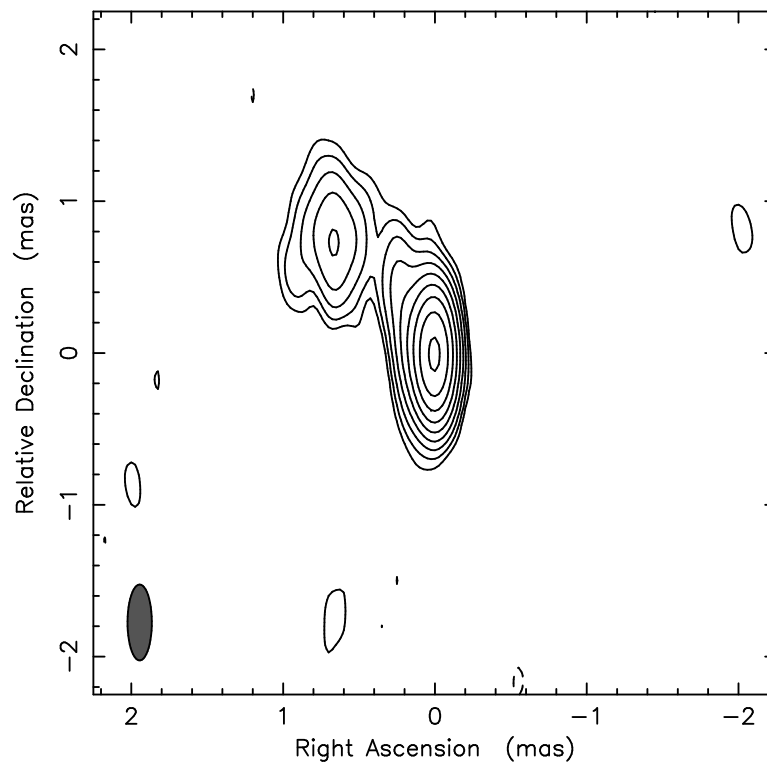


**Figure 1.** The 43-GHz image of CTD 135 based on VLBA data obtained on 18 January 2016 [27]. The peak brightness is  $877 \text{ mJy beam}^{-1}$ , the lowest contours are drawn at  $\pm 3 \text{ mJy beam}^{-1}$  and the positive contour levels increase by a factor of 2. The half-power width of the elliptical Gaussian restoring beam is  $0.5 \text{ mas} \times 0.16 \text{ mas}$  with the major axis oriented in the north–south direction, as displayed in the bottom left corner.

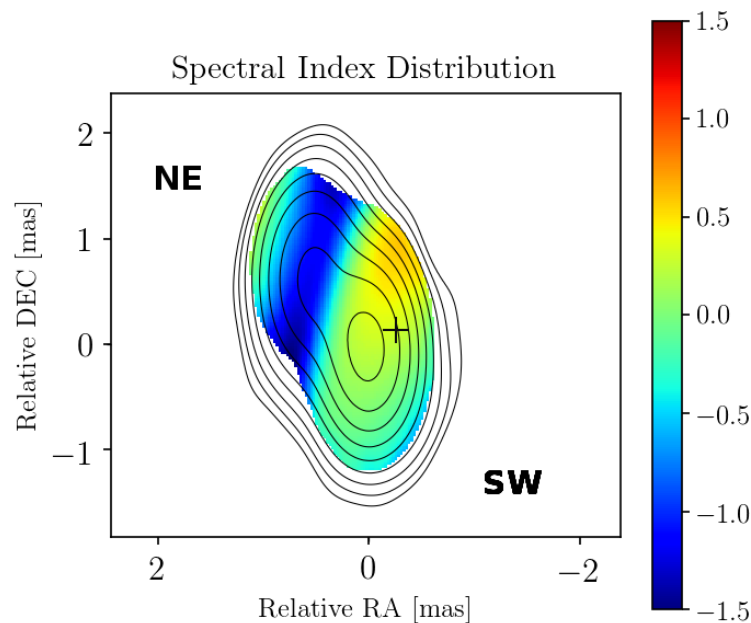


**Figure 2.** Spectral index map of CTD 135 between 15 and 43 GHz frequencies, based on VLBA images obtained nearly simultaneously, within 1 month in 2015 December and 2016 January. The half-power width of the common elliptical Gaussian restoring beam is  $1.0 \text{ mas} \times 0.5 \text{ mas}$  with the major axis oriented in the north–south direction. The contours, starting at  $2 \text{ mJy beam}^{-1}$  and increasing by a factor of 2, show the 15-GHz brightness distribution. The peak intensity is  $726 \text{ mJy beam}^{-1}$ . The spectral index values are indicated by colours with the scale displayed in the right. The cross marks the relative position of the *Gaia* optical source, its size indicates the  $1\text{-}\sigma$  formal uncertainties.

Both the 15- and 43-GHz images were convolved with a common restoring beam, using visibility data in the same ranges of VLBA baselines expressed in the units of wavelength. Both naturally weighted images were sampled with the same cell size ( $0.025 \text{ mas}$ ). The on-source integration times were  $\sim 54 \text{ min}$  and  $\sim 20 \text{ min}$  at 15 and 43 GHz, respectively. The typical error of the spectral index in the central regions of the map is estimated as 0.1, considering also the flux density calibration uncertainties. It is clear from Figure 2 that the SW component has a flat spectrum ( $\alpha \approx 0$ ), characteristic of a synchrotron self-absorbed core, while the NE component has a steep spectrum ( $\alpha < -0.5$ ) expected for an optically thin jet feature. This is evidence for a blazar with a core–jet structure.

Another way to assess the spectral properties of the source is to characterize the brightness distribution of the core and the jet by fitting circular Gaussian components to the visibility data, and calculate the two-point spectral index from the component flux densities at 15 and 43 GHz. The fitted core (SW) flux density is  $S_{\text{core}}^{15} = 755 \pm 39 \text{ mJy}$  and  $S_{\text{core}}^{43} = 925 \pm 48 \text{ mJy}$  at 15 and 43 GHz, respectively. The flux densities obtained for the jet component (NE) are  $S_{\text{jet}}^{15} = 422 \pm 33 \text{ mJy}$  and  $S_{\text{jet}}^{43} = 178 \pm 15 \text{ mJy}$ . Note that [27] fitted a core and two jet components to the same data but our choice of the simpler model is dictated by the 15-GHz data set where the additional inner jet component remains unresolved. The two-point spectral indices are  $\alpha_{\text{core}} = 0.20 \pm 0.10$  and  $\alpha_{\text{jet}} = -0.84 \pm 0.16$ .

The brightness temperature estimated for the core (i.e., the SW feature) at 43 GHz is  $T_B \gtrsim 4 \times 10^{11} \text{ K}$  [27]. This exceeds the equipartition value [30] by almost an order of magnitude, indicating a relativistically beamed jet with a Doppler factor  $\delta \gtrsim 9 - 10$ . Again, this is not expected for a CSO with a misaligned jet.

## 2.2. Spectral Energy Distribution

The broad-band SED constructed for CTD 135 by [22] using literature data spanning multiple electromagnetic wavebands from radio to  $\gamma$ -rays can be well-fitted with the two-zone leptonic radiation model usually applied for blazars, assuming a small jet inclination angle. Remarkably, [22] estimate a Doppler factor  $\delta = 10.8$  for the core region. This is consistent with the value deduced from the 43-GHz VLBI observations [27]. For their SED fit, [22] assumed a compact core component and a homogeneous extended (5 mas) spherical emission region. Instead of the CSO, they suggest that the extended  $\gamma$ -ray structure is attributed to symmetric bubbles surrounding the AGN.

## 2.3. Radio Variability

As noted already by [15], long-term non-simultaneous total flux density measurements of CTD 135, as well as archival VLBI flux density measurements, indicate significant variability at all frequencies above  $\sim 1$  GHz. They attributed this to the variability of the putative central core component, of which the existence, however, is not confirmed by the new 43-GHz VLBI imaging [27]. The core is highly self-absorbed and relatively weak at frequencies below 15 GHz. It is therefore possible that the radio flux density variability is mostly associated with the NE (jet) component at lower frequencies and the SW (core) component at high frequencies.

In their study on CSO identification problems, [18] also mention CTD 135 as an object exhibiting blazar-like flux density variability. By accepting that this is a beamed core-jet source (Figure 2), the variability properties can indeed be naturally explained.

## 2.4. $\gamma$ -ray Variability

CTD 135 is variable not only in the radio but in  $\gamma$ -rays as well, according to  $\sim 11$  yr of *Fermi*/LAT measurements thoroughly analysed by [22]. The authors label the source as extremely variable in the  $\gamma$ -ray band, and even claim the detection of a  $\sim 460$ -d quasi-periodic oscillation (QPO) in the light curve of CTD 135. The variability, together with the high  $\gamma$ -ray luminosity, indicate Doppler-boosted radiation [22], a characteristic signature of blazars but not CSOs. The  $\gamma$ -ray flux may have two origins. On the one hand, a synchrotron self-Compton core component is responsible for the  $\gamma$ -ray QPO and the high-frequency radio variability. The other contribution is a shocked component due to the interaction of the jet with the interstellar medium in the NE feature. The latter would explain the ‘extended’  $\gamma$ -ray emission component included in the SED fit [22].

## 2.5. Infrared Colours and Variability

CTD 135 was detected by the *Wide-field Infrared Survey Explorer* (WISE) [31] in all four of its wavebands, at  $3.4\ \mu\text{m}$  (W1),  $4.6\ \mu\text{m}$  (W2),  $12\ \mu\text{m}$ , and  $22\ \mu\text{m}$  (W4) [32]. Its infrared colours place it in the  $\gamma$ -ray blazar strip on the WISE colour-colour diagram [33]. Additionally, it is listed as a likely blazar in the second WISE Blazar-like Radio-Loud Sources (WIBRaLS2) catalogue [34].

The WISE satellite, after the completion of its original mission, continued its all-sky survey in the framework of the NEOWISE (Near-Earth Object WISE) project [35] and afterwards as the NEOWISE Reactivation mission. Because of the depleted cooling material, in the prolonged projects the satellite remained operational only in the two shortest-wavelength (mid-infrared) bands, W1 and W2.

We downloaded the WISE single exposure data (<http://irsa.ipac.caltech.edu/Missions/wise.html>, accessed: 2 February 2022). Following the instructions of the Exploratory Supplement Series ([https://wise2.ipac.caltech.edu/docs/release/allwise/expsup/sec3\\_2.html](https://wise2.ipac.caltech.edu/docs/release/allwise/expsup/sec3_2.html), accessed: 2 February 2022), we discarded measurements of bad quality. These involved data (25 measurement points) that have a profile-fit goodness value of  $\geq 3$  in either the W1 or W2 bands, indicating that a point-source model was not able to adequately describe the data (e.g.,



an image artifact was affecting the measurements). Then, we converted the magnitude values to flux densities and constructed the light curves shown in Figures 3 and 4.

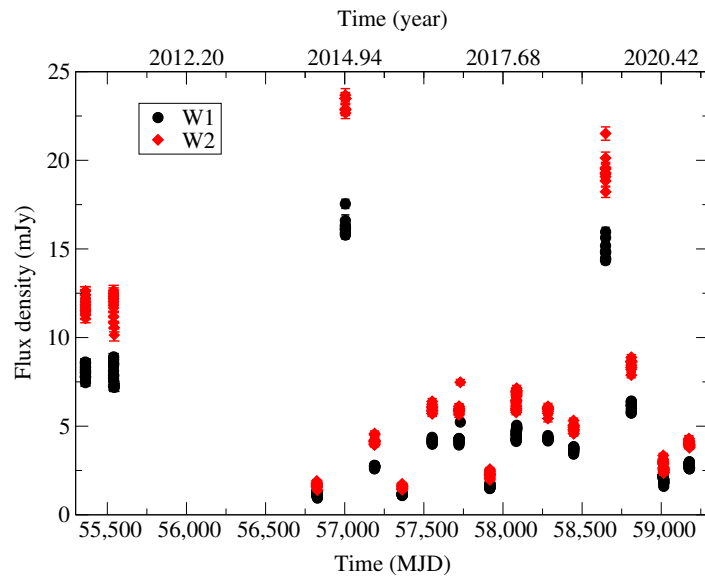


**Figure 3.** WISE light curve of CTD 135 at  $3.4\ \mu\text{m}$  (W1) and  $4.6\ \mu\text{m}$  (W2), with black and red symbols, respectively.

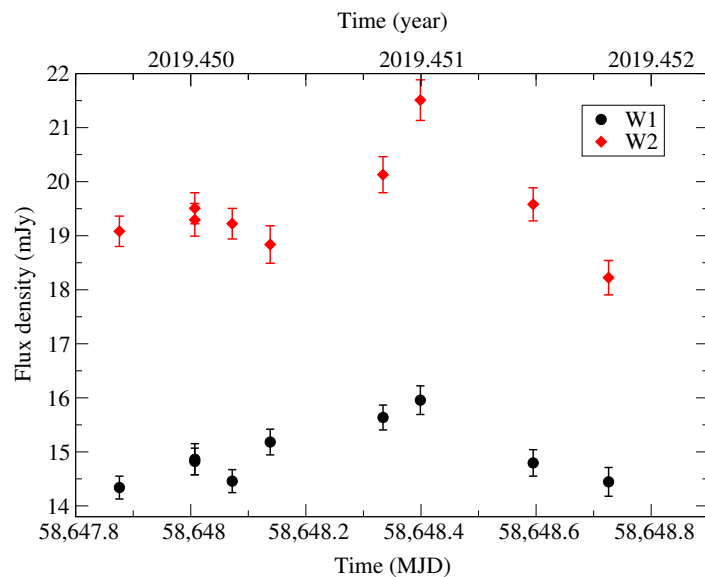


**Figure 4.** A zoom-in to the WISE light curve of CTD 135 at the mission phase 13 in Figure 3 at  $3.4\ \mu\text{m}$  (W1) and  $4.6\ \mu\text{m}$  (W2), with black and red symbols, respectively.

CTD 135 shows significant variation in its long-term infrared light curve in both bands (Figure 3). Notably, the two epochs when its flux density reached the highest values, in December 2014, near Modified Julian Date (MJD) 57,000, and in June 2019 (MJD  $\approx$  58,650), coincide with epochs of  $\gamma$ -ray brightening according to the light curve taken by the *Fermi* satellite [22].

In some mission phases, significant variability within a time span as short as a few days can also be seen in the infrared bands. An example is shown in Figure 4. Through causality argument, flux density change on a short time-scale implies small size for the emitting region responsible for the variability (e.g., [36]). Thus, the variable infrared emission cannot originate from extended regions of the dusty torus or the host galaxy of CTD 135. A coherent outburst lasting for  $\sim 0.5$  d in the observed frame (Figure 4), if corrected for the cosmological time dilation, implies an emission region within  $0.5/(1+z)$  light days, or  $\sim 0.0002$  pc. A statistical study of the short-term infrared variability of *Fermi*-detected blazars by [37] clearly showed the jet origin of their infrared emission observed in the *WISE* bands.

In summary, the infrared characteristics (colour and variability) of CTD 135 make it similar to the beamed blazar sources.

## 2.6. VLBI and Gaia Positions

The accurate equatorial coordinates of CTD 135 in the radio are right ascension  $RA_{\text{VLBI}} = 22^{\text{h}}36^{\text{m}}22.4708467^{\text{s}}$  and declination  $DEC_{\text{VLBI}} = 28^{\circ}28'57.412755''$  in the catalogue of the 3rd realization of the VLBI-derived International Celestial Reference Frame [38]. Here we consider the 32-GHz position (X/Ka-band solution (<https://hpiers.obspm.fr/icrs-pc/newwww/icrf/icrf3xka.txt>, accessed: 2 February 2022)) because we use high-frequency images for the spectral index map (Figure 2). The formal errors are 0.07 mas and 0.08 mas for RA and DEC, respectively. In the optical, the most recent *Gaia* Early Data Release 3 (EDR3) [39] lists (<https://gea.esac.esa.int/archive/>, accessed: 2 February 2022) the object with right ascension  $RA_{\text{Gaia}} = 22^{\text{h}}36^{\text{m}}22.4708284^{\text{s}}$  and declination  $DEC_{\text{Gaia}} = 28^{\circ}28'57.412946''$  (J2000), with 0.1 mas formal uncertainty in both coordinates and insignificant astrometric excess noise. The radio–optical coordinate differences,  $\Delta RA = (0.31 \pm 0.12)$  mas and  $\Delta DEC = (-0.19 \pm 0.13)$  mas, are quite small, well within the values generally found between ICRF3 and *Gaia* EDR3 [40]. The optical position with the above error bars is marked with a cross in Figure 2. Although it is very close to the brightness peak in the SW core, given the small overall angular extent of this radio source ( $<2$  mas), the astrometric test is rather inconclusive regarding the CSO versus blazar classification. Especially because radio–optical positional offsets of up to  $\sim 1$  mas are ubiquitous in radio AGN, typically along the pc-scale jet direction [20].

## 3. Summary—The Classification of CTD 135 as a Blazar

In their recent publication, [18] used CTD 135 as one of the examples for potential CSO candidates, based on its radio spectrum composed of non-simultaneous flux density measurements, indicating strong variability. Indeed, as it is suggested by independent observational evidence collected in Section 2, CTD 135 shares its properties with blazars, AGN with relativistic jets pointed towards the observer. In particular, the existence of the compact flat/inverted-spectrum SW component (Figure 2), clearly resolved with VLBI at 43 GHz and characterised by high brightness temperature [27], the highly variable  $\gamma$ -ray and mid-infrared emission, and the broad-band SED indicating Doppler-boosted emission [22] are all against the CSO classification tentatively proposed by [15].

We find it important to point out that CTD 135 did not pass the scrutiny of a detailed multi-band investigation as a CSO candidate, and it is in fact *not* a CSO. While being labeled as a “CSO candidate”, this AGN unfortunately already started its doubtful career in the literature as a (misclassified) rare  $\gamma$ -ray-emitting radio AGN with misaligned compact symmetric jets [12, 22,41]. Following our study based on essential new observational data, we suggest removing CTD 135 from the list of compact symmetric objects.

Because of the difficulties in finding young  $\gamma$ -ray-emitting AGN [42], it is of high importance to verify the CSO nature of each new candidate proposed. The multi-waveband diagnostic methods applied here for the case of CTD 135 could be useful for detailed studies of other potential  $\gamma$ -ray



CSOs as well. The investigations of *WISE* infrared variability and the radio–optical positional offsets based on VLBI and *Gaia* measurements in particular could offer a novel approach to this work.

**Author Contributions:** Conceptualization, S.F.; methodology, S.F., K.É.G., T.A.; writing—original draft preparation, S.F.; writing—review and editing, K.É.G., T.A.; visualization, K.É.G. All authors have read and agreed to the published version of the manuscript.

**Funding:** This research was funded by the Hungarian National Research, Development and Innovation Office (NKFIH), grant numbers OTKA K134213 and 2018-2.1.14-TÉT-CN-2018-00001.

**Data Availability Statement:** Calibrated VLBI data used for creating the images are available from the Astrogéo Center database (<http://www.astrogéo.org>, accessed: 2 February 2022). *WISE* data used for creating the light curve are available from the NASA/IPAC Infrared Science Archive (<https://irsa.ipac.caltech.edu/Missions/wise.html>, accessed: 2 February 2022).

**Acknowledgments:** We thank the four anonymous referees for their comments and suggestions. This research has made use of data from the MOJAVE database that is maintained by the MOJAVE team [23]. We acknowledge the use of archival calibrated VLBI data from the Astrogéo Center database maintained by Leonid Petrov. This publication makes use of data products from the *WISE*, which is a joint project of the University of California, Los Angeles, and the Jet Propulsion Laboratory/California Institute of Technology, funded by the National Aeronautics and Space Administration.

**Conflicts of Interest:** The authors declare no conflict of interest.

## Abbreviations

The following abbreviations are used in this manuscript:

CSO	compact symmetric object
EDR3	<i>Gaia</i> Early Data Release 3
FSRQ	flat-spectrum radio quasar
LAT	Large Area Telescope (of the <i>Fermi</i> satellite)
mas	milliarcsecond
MJD	Modified Julian Date
MSO	medium-sized symmetric object
MOJAVE	Monitoring of Jets in Active Galactic Nuclei with VLBA Experiments
QPO	quasi-periodic oscillation
SED	spectral energy distribution
VLBA	Very Long Baseline Array
VLBI	very long baseline interferometry
WISE	Wide-field Infrared Survey Explorer

## References

1. Wilkinson, P.N.; Polatidis, A.G.; Readhead, A.C.S.; Xu, W.; Pearson, T.J. Two-sided Ejection in Powerful Radio Sources: The Compact Symmetric Objects. *Astrophys. J. Lett.* **1994**, *432*, L87. doi:10.1086/187518.
2. Urry, C.M.; Padovani, P. Unified Schemes for Radio-Loud Active Galactic Nuclei. *Publ. Astron. Soc. Pac.* **1995**, *107*, 803. doi:10.1086/133630.
3. Fanti, C.; Fanti, R.; Dallacasa, D.; Schilizzi, R.T.; Spencer, R.E.; Stanghellini, C. Are compact steep-spectrum sources young? *Astron. Astrophys.* **1995**, *302*, 317.
4. Owsianik, I.; Conway, J.E. First detection of hotspot advance in a Compact Symmetric Object. Evidence for a class of very young extragalactic radio sources. *Astron. Astrophys.* **1998**, *337*, 69–79.
5. Taylor, G.B.; Marr, J.M.; Pearson, T.J.; Readhead, A.C.S. Kinematic Age Estimates for Four Compact Symmetric Objects from the Pearson-Readhead Survey. *Astrophys. J.* **2000**, *541*, 112–119. doi:10.1086/309428.
6. An, T.; Baan, W.A. The Dynamic Evolution of Young Extragalactic Radio Sources. *Astrophys. J.* **2012**, *760*, 77. doi:10.1088/0004-637X/760/1/77.
7. Abdollahi, S.; Acero, F.; Ackermann, M.; Ajello, M.; Atwood, W.B.; Axelsson, M.; Baldini, L.; Ballet, J.; Barbiellini, G.; Bastieri, D.; et al. Fermi Large Area Telescope Fourth Source Catalog. *Astrophys. J. Suppl. Ser.* **2020**, *247*, 33. doi:10.3847/1538-4365/ab6bcb.
8. Stawarz, Ł.; Ostorero, L.; Begelman, M.C.; Moderski, R.; Kataoka, J.; Wagner, S. Evolution of and High-Energy Emission from GHz-Peaked Spectrum Sources. *Astrophys. J.* **2008**, *680*, 911–925. doi:10.1086/587781.
9. Kino, M.; Ito, H.; Kawakatu, N.; Nagai, H. New prediction of extragalactic GeV  $\gamma$ -ray emission from radio lobes of young AGN jets. *Mon. Not. R. Astron. Soc.* **2009**, *395*, L43–L47. doi:10.1111/j.1745-3933.2009.00638.x.
10. Migliori, G.; Siemiginowska, A.; Kelly, B.C.; Stawarz, Ł.; Celotti, A.; Begelman, M.C. Jet Emission in Young Radio Sources: A Fermi Large Area Telescope Gamma-Ray View. *Astrophys. J.* **2014**, *780*, 165. doi:10.1088/0004-637X/780/2/165.
11. An, T.; Lao, B.Q.; Zhao, W.; Mohan, P.; Cheng, X.P.; Cui, Y.Z.; Zhang, Z.L. Parsec-scale jet properties of the gamma-ray quasar 3C 286. *Mon. Not. R. Astron. Soc.* **2017**, *466*, 952–959. doi:10.1093/mnras/stw2887.
12. O’Dea, C.P.; Saikia, D.J. Compact steep-spectrum and peaked-spectrum radio sources. *Astron. Astrophys. Rev.* **2021**, *29*, 3. doi:10.1007/s00159-021-00131-w.
13. Migliori, G.; Siemiginowska, A.; Sobolewska, M.; Loh, A.; Corbel, S.; Ostorero, L.; Stawarz, Ł. First Detection in Gamma-Rays of a Young Radio Galaxy: Fermi-LAT Observations of the Compact Symmetric Object PKS 1718-649. *Astrophys. J. Lett.* **2016**, *821*, L31. doi:10.3847/2041-8205/821/2/L31.
14. Principe, G.; Migliori, G.; Johnson, T.J.; D’Ammando, F.; Giroletti, M.; Orienti, M.; Stanghellini, C.; Taylor, G.B.; Torresi, E.; Cheung, C.C. NGC 3894: A young radio galaxy seen by Fermi-LAT. *Astron. Astrophys.* **2020**, *635*, A185. doi:10.1051/0004-6361/201937049.
15. An, T.; Cui, Y.Z.; Gabányi, K.É.; Frey, S.; Baan, W.A.; Zhao, W. Radio properties of the  $\gamma$ -ray emitting CSO candidate 2234+282. *Astron. Nachr.* **2016**, *337*, 65. doi:10.1002/asna.201512266.
16. Shaw, M.S.; Romani, R.W.; Cotter, G.; Healey, S.E.; Michelson, P.F.; Readhead, A.C.S.; Richards, J.L.; Max-Moerbeck, W.; King, O.G.; Potter, W.J. Spectroscopy of Broad-line Blazars from 1LAC. *Astrophys. J.* **2012**, *748*, 49. doi:10.1088/0004-637X/748/1/49.
17. Phillips, R.B.; Mutel, R.L. On symmetric structure in compact radio sources. *Astron. Astrophys.* **1982**, *106*, 21–24.

18. Readhead, A.C.S.; Kiehlmann, S.; Lister, M.L.; O'Neill, S.; Pearson, T.J.; Sheldahl, E.; Siemiginowska, A.; Taylor, G.B.; Wilkinson, P.N. What defines a compact symmetric object? A carefully vetted sample of compact symmetric objects. *Astron. Nachr.* **2021**, *342*, 1185–1190. doi:10.1002/asna.20210049.
19. Gaia Collaboration; Prusti, T.; de Bruijne, J.H.J.; Brown, A.G.A.; Vallenari, A.; Babusiaux, C.; Bailer-Jones, C.A.L.; Bastian, U.; Biermann, M.; Evans, D.W.; et al. The Gaia mission. *Astron. Astrophys.* **2016**, *595*, A1. doi:10.1051/0004-6361/201629272.
20. Kovalev, Y.Y.; Petrov, L.; Plavin, A.V. VLBI-Gaia offsets favor parsec-scale jet direction in active galactic nuclei. *Astron. Astrophys.* **2017**, *598*, L1. doi:10.1051/0004-6361/201630031.
21. Krezinger, M.; Frey, S.; An, T.; Jaiswal, S.; Zhang, Y. J1110+4817—A compact symmetric object candidate revisited. *Mon. Not. R. Astron. Soc.* **2020**, *496*, 1811–1818. doi:10.1093/mnras/staa1669.
22. Gan, Y.Y.; Zhang, H.M.; Zhang, J.; Yang, X.; Yi, T.F.; Liang, Y.F.; Liang, E.W. Highly variable  $\gamma$ -ray emission of CTD 135 and implications for its compact symmetric structure. *Res. Astron. Astrophys.* **2021**, *21*, 201. doi:10.1088/1674-4527/21/8/201.
23. Lister, M.L.; Aller, M.F.; Aller, H.D.; Hodge, M.A.; Homan, D.C.; Kovalev, Y.Y.; Pushkarev, A.B.; Savolainen, T. MOJAVE. XV. VLBA 15 GHz Total Intensity and Polarization Maps of 437 Parsec-scale AGN Jets from 1996 to 2017. *Astrophys. J. Suppl. Ser.* **2018**, *234*, 12. doi:10.3847/1538-4365/aa9c44.
24. Lister, M.L.; Aller, M.F.; Aller, H.D.; Homan, D.C.; Kellermann, K.I.; Kovalev, Y.Y.; Pushkarev, A.B.; Richards, J.L.; Ros, E.; Savolainen, T. MOJAVE: XIII. Parsec-scale AGN Jet Kinematics Analysis Based on 19 years of VLBA Observations at 15 GHz. *Astron. J.* **2016**, *152*, 12. doi:10.3847/0004-6256/152/1/12.
25. Lister, M.L.; Homan, D.C.; Kellermann, K.I.; Kovalev, Y.Y.; Pushkarev, A.B.; Ros, E.; Savolainen, T. Monitoring Of Jets in Active Galactic Nuclei with VLBA Experiments. XVIII. Kinematics and Inner Jet Evolution of Bright Radio-loud Active Galaxies. *Astrophys. J.* **2021**, *923*, 30. doi:10.3847/1538-4357/ac230f.
26. Hodge, M.A.; Lister, M.L.; Aller, M.F.; Aller, H.D.; Kovalev, Y.Y.; Pushkarev, A.B.; Savolainen, T. MOJAVE XVI: Multiepoch Linear Polarization Properties of Parsec-scale AGN Jet Cores. *Astrophys. J.* **2018**, *862*, 151. doi:10.3847/1538-4357/aac2f.
27. Cheng, X.P.; An, T.; Frey, S.; Hong, X.Y.; He, X.; Kellermann, K.I.; Lister, M.L.; Lao, B.Q.; Li, X.F.; Mohan, P.; et al. Compact Bright Radio-loud AGNs. III. A Large VLBA Survey at 43 GHz. *Astrophys. J. Suppl. Ser.* **2020**, *247*, 57. doi:10.3847/1538-4365/ab791f.
28. Shepherd, M.C.; Pearson, T.J.; Taylor, G.B. DIFMAP: An interactive program for synthesis imaging. *Bull. Am. Astron. Soc.* **1994**, *26*, 987–989.
29. Kim, J.Y.; Trippe, S. VIMAP: An Interactive Program Providing Radio Spectral Index Maps of Active Galactic Nuclei. *J. Korean Astron. Soc.* **2014**, *47*, 195–199. doi:10.5303/JKAS.2014.47.5.195.
30. Readhead, A.C.S. Equipartition Brightness Temperature and the Inverse Compton Catastrophe. *Astrophys. J.* **1994**, *426*, 51. doi:10.1086/174038.
31. Wright, E.L.; Eisenhardt, P.R.M.; Mainzer, A.K.; Ressler, M.E.; Cutri, R.M.; Jarrett, T.; Kirkpatrick, J.D.; Padgett, D.; McMillan, R.S.; Skrutskie, M.; et al. The Wide-field Infrared Survey Explorer (WISE): Mission Description and Initial On-orbit Performance. *Astron. J.* **2010**, *140*, 1868–1881. doi:10.1088/0004-6256/140/6/1868.
32. Cutri, R.M.; Wright, E.L.; Conrow, T.; Fowler, J.W.; Eisenhardt, P.R.M.; Grillmair, C.; Kirkpatrick, J.D.; Masci, F.; McCallon, H.L.; Wheelock, S.L.; et al. VizieR Online Data Catalog: AllWISE Data Release (updated version, 16-Feb-2021). *VizieR Online Data Catalog* **2021**, II/328.
33. Massaro, F.; D'Abrusco, R.; Ajello, M.; Grindlay, J.E.; Smith, H.A. Identification of the Infrared Non-thermal Emission in Blazars. *Astrophys. J. Lett.* **2011**, *740*, L48. doi:10.1088/2041-8205/740/2/L48.
34. D'Abrusco, R.; Álvarez Crespo, N.; Massaro, F.; Campana, R.; Chavushyan, V.; Landoni, M.; La Franca, F.; Masetti, N.; Milisavljevic, D.; Paggi, A.; et al. Two New Catalogs of Blazar Candidates in the WISE Infrared Sky. *Astrophys. J. Suppl. Ser.* **2019**, *242*, 4. doi:10.3847/1538-4365/ab16f4.
35. Mainzer, A.; Bauer, J.; Cutri, R.M.; Grav, T.; Masiero, J.; Beck, R.; Clarkson, P.; Conrow, T.; Dailey, J.; Eisenhardt, P.; et al. Initial Performance of the NEOWISE Reactivation Mission. *Astrophys. J.* **2014**, *792*, 30. doi:10.1088/0004-637X/792/1/30.
36. Jiang, N.; Zhou, H.Y.; Ho, L.C.; Yuan, W.; Wang, T.G.; Dong, X.B.; Jiang, P.; Ji, T.; Tian, Q. Rapid Infrared Variability of Three Radio-loud Narrow-line Seyfert 1 Galaxies: A View from the Wide-field Infrared Survey Explorer. *Astrophys. J. Lett.* **2012**, *759*, L31. doi:10.1088/2041-8205/759/2/L31.
37. Anjum, A.; Stalin, C.S.; Rakshit, S.; Gudennavar, S.B.; Durgapal, A. Mid-infrared variability of  $\gamma$ -ray emitting blazars. *Mon. Not. R. Astron. Soc.* **2020**, *494*, 764–774. doi:10.1093/mnras/staa771.
38. Charlot, P.; Jacobs, C.S.; Gordon, D.; Lambert, S.; de Witt, A.; Böhm, J.; Fey, A.L.; Heinkelmann, R.; Skurikhina, E.; Titov, O.; et al. The third realization of the International Celestial Reference Frame by very long baseline interferometry. *Astron. Astrophys.* **2020**, *644*, A159. doi:10.1051/0004-6361/202038368.
39. Gaia Collaboration; Brown, A.G.A.; Vallenari, A.; Prusti, T.; de Bruijne, J.H.J.; Babusiaux, C.; Biermann, M.; Creevey, O.L.; Evans, D.W.; Eyer, L.; et al. Gaia Early Data Release 3. Summary of the contents and survey properties. *Astron. Astrophys.* **2021**, *649*, A1. doi:10.1051/0004-6361/202039657.

- 
40. Liu, N.; Lambert, S.B.; Charlot, P.; Zhu, Z.; Liu, J.C.; Jiang, N.; Wan, X.S.; Ding, C.Y. Comparison of multifrequency positions of extragalactic sources from ICRF3 and Gaia EDR3. *Astron. Astrophys.* **2021**, *652*, A87. doi:10.1051/0004-6361/202038179.
  41. Schinzel, F.K.; Petrov, L.; Taylor, G.B.; Edwards, P.G. Radio Follow-up on All Unassociated Gamma-Ray Sources from the Third Fermi Large Area Telescope Source Catalog. *Astrophys. J.* **2017**, *838*, 139. doi:10.3847/1538-4357/aa6439.
  42. D'Ammando, F.; Orienti, M.; Giroletti, M.; Fermi Large Area Telescope Collaboration. The Fermi-LAT view of young radio sources. *Astron. Nachr.* **2016**, *337*, 59. doi:10.1002/asna.201512265.